

1.55- μm Vertical-Cavity Laser Arrays for Wavelength-Division Multiplexing

Adil Karim, *Student Member, IEEE*, Joachim Piprek, *Senior Member, IEEE*, Patrick Abraham, *Senior Member, IEEE*, Dan Lofgreen, *Student Member, IEEE*, Yi-Jen Chiu, *Member, IEEE*, and John E. Bowers, *Fellow, IEEE*

Abstract—We report on the fabrication and operation of the first electrically pumped 1.55- μm vertical-cavity laser array for wavelength-division-multiplexing applications. The array consisted of four channels operating between 1509 and 1524 nm. Wafer bonding was used to integrate GaAs–AlGaAs distributed Bragg reflectors with an InP–InGaAsP active region.

Index Terms—Distributed Bragg reflectors, semiconductor lasers, surface-emitting lasers, vertical-cavity lasers, wafer bonding.

I. INTRODUCTION

VERTICAL-CAVITY surface-emitting lasers (VCSELs) in the 1.55- μm wavelength region are attractive sources for optical networks. These devices offer many advantages compared to edge-emitting lasers, the most prominent of which is compatibility with low-cost wafer-scale fabrication and testing. Additional advantages include low power consumption, high fiber coupling efficiency, single-mode operation and the capacity for producing two-dimensional arrays on wafer. High-performance devices have been fabricated using buried tunnel junctions [1], antimonide mirrors [2] and metamorphic growth [3], [4]. However, the main limitation to realizing commercial devices has been high-temperature performance. The most commonly used material system for 1.55- μm emission is InP–InGaAsP, which is limited in VCSEL applications by low refractive index contrast, low thermal conductivity, high intervalence band absorption, and high Auger recombination rates. The lack of a robust aperturing technique on InP similar to the lateral oxidation of AlGaAs on GaAs has also slowed the rate of progress in long-wavelength VCSEL development. The best high-temperature results to date have been achieved using wafer bonded GaAs–AlGaAs distributed Bragg reflectors (DBRs) in both electrically pumped [5] and optically pumped [6] designs. The high thermal conductivity and index contrast available in the GaAs–AlGaAs material system make it an attractive choice for fabricating long-wavelength VCSEL DBRs. The wafer bonding technique allows for the integration of materials with different lattice constants, such as GaAs and InP, that are difficult to integrate epitaxially. In VCSELs, wafer

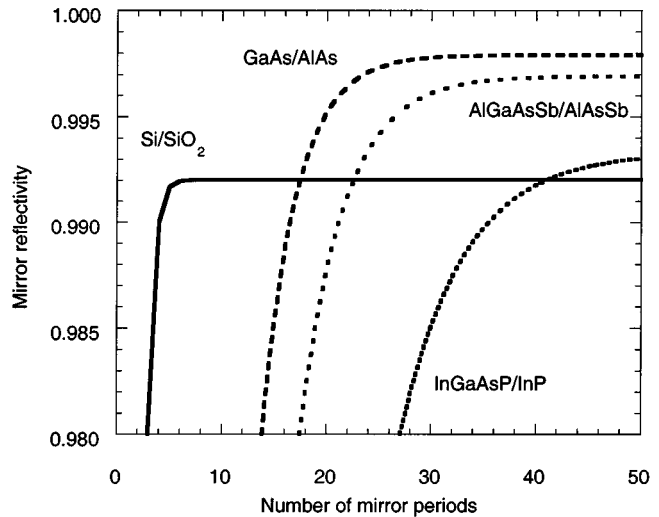


Fig. 1. DBR reflectivity versus the number of mirror periods for different material systems.

bonding allows for processing prior to laser cavity formation. In this work, multiple laser cavities with different wavelengths were defined prior to bonding the active region and DBRs, creating a four-channel VCSEL array for wavelength division multiplexing (WDM).

II. DISTRIBUTED BRAGG REFLECTORS (DBRs)

The principal obstacle in long-wavelength VCSEL development has been the lack of high-quality DBRs that can be integrated with InP-based active regions. DBRs with high thermal conductivity, high reflectivity, and, in the case of current injection through the DBR, high electrical conductivity have proven difficult to fabricate on InP. These considerations must be balanced in order to optimize VCSEL performance. Fig. 1 compares reflectivity versus number of DBR periods for four different 1550-nm VCSEL mirrors. The four mirror systems shown are a-Si–SiO₂, GaAs–AlAs, AlGaAsSb–AlAsSb, and InGaAsP–InP. The a-Si–SiO₂ DBR reaches peak reflectivity with a small number of mirror periods, but this value is limited by absorption in the deposited amorphous layers. These characteristics are typical of deposited dielectric DBRs. The other mirror systems shown are grown epitaxially. These DBRs require a higher number of mirror periods to reach the reflectivities needed in VCSELs ($\approx 99\%$), but are capable of reaching higher peak reflectivities than dielectric DBRs due to lower material absorption. The exact reflectivity of a particular DBR depends on the exact alloy composition and doping scheme

Manuscript received November 29, 2000; revised March 23, 2001. This work was supported by the Defense Advanced Research Projects Agency (DARPA) via the Heterogeneous Optoelectronics Technology Center (HOTC).

A. Karim and P. Abraham were with the University of California at Santa Barbara, Santa Barbara, CA 93106 USA, now they are with Agility Communications, Santa Barbara, CA 93117 USA (e-mail: akarim@agility.com).

J. Piprek, D. Lofgreen, Y.-J. Chiu, and J. E. Bowers are with the University of California at Santa Barbara, Santa Barbara, CA 93106 USA.

Publisher Item Identifier S 1077-260X(01)08026-1.

TABLE I
OPTICAL AND THERMAL PROPERTIES OF 1.55- μm VCSEL DBRs

DBR Composition	n_1	κ_1	n_2	κ_2	N for 99%	R_{th}
GaAs/AlAs	3.37	0.44	2.89	0.91	16	57.5
InGaAsP (1.4 μm)/InP	3.45	0.045	3.17	0.68	28	174.7
AlGaAsSb/AlAsSb	3.50	0.062	3.10	0.057	16	627.5
AlInGaAs/AlInAs	3.47	0.045	3.21	0.045	30	1549.2
a-Si/SiO ₂	3.6	0.026	1.45	0.012	4	936.0
a-Si/Al ₂ O ₃	3.6	0.026	1.74	0.36	5	65.8

used. The InGaAsP–InP system is the most commonly grown on InP, but is limited by low index contrast. Thick mirrors are required to reach reasonable reflectivity levels, leading to significant propagation losses. The AlGaAsSb–AlAsSb system has been studied recently for DBR applications on InP [7], [8]. This system features higher index contrast than InGaAsP–InP DBRs. GaAs–AlAs DBRs have slightly higher index contrast than AlGaAsSb–AlAsSb DBRs, but have a significantly higher thermal conductivity. Due to the lattice mismatch between GaAs and InP, GaAs–AlAs DBRs must be wafer bonded to [9], [10] or metamorphically grown on [11] InP-based active regions.

The thermal conductivity of a DBR is also an important parameter. DBRs must be able to effectively dissipate heat from resistive and lasing processes. Heat dissipation is critical in long-wavelength VCSELs due to the low characteristic temperatures of InP-based active regions. Dielectric mirrors usually have low thermal conductivities, though recent device results have shown significant improvement with top-down mounting [12], [13]. The thermal conductivity of epitaxial mirrors depends greatly on alloy composition. Ternary and quaternary alloys have substantially lower thermal conductivities than binary mirrors, due to alloy scattering [14]. Table I summarizes optical and thermal data for 1550-nm VCSEL DBRs. The values for n_1 and n_2 refer to the indices of refraction for the first and second mirror materials listed in each row. The thermal conductivities of these materials are given by κ_1 and κ_2 in W/cm \cdot K. The next column shows N , the number of mirror periods required for 99% reflectivity for each DBR combination. The thermal resistance of a 99% reflective DBR with an area of 1000 μm^2 is given in the final column by R_{th} in K/W. The thermal resistance of a particular mirror stack is calculated by dividing the required mirror length by the area given above and the effective thermal conductivity of the mirror material. These calculations only include one-dimensional (1-D) heat flow, but give a qualitative idea of the relative thermal resistances of different DBR materials. The exact thermal resistance of a VCSEL depends on a number of factors, including the active region layer structure, device size, and heat sinking.

The mature growth technology, high reflectivity, and low thermal resistance of GaAs based DBRs make them an attractive choice for long-wavelength VCSELs. Lateral oxidation [15], [16] of these DBRs for mode and current confinement can dramatically improve device performance compared to unapertured devices. The advantages of GaAs-based DBRs

have led to a number of efforts to integrate these DBRs with long-wavelength InP-based active regions.

III. WAFER BONDING AND DEVICE STRUCTURE

Wafer bonding of GaAs DBRs and InP-based active regions has consistently produced high-performance long-wavelength VCSELs, including the first electrically pumped devices to operate in CW at room temperature [17] and with submilliampere threshold currents [18]. Details of the wafer bonding technique have been published previously [9].

Wavelength-division multiplexing (WDM) has enabled a dramatic increase in the data capacity of optical networks. However, assembling and packaging discrete lasers with different wavelengths is expensive and time-consuming. Multiple-wavelength arrays of vertical-cavity lasers are desirable sources for WDM systems due to reduced production costs and other advantages cited earlier. The simple testing and packaging procedures for 1-D and two-dimensional (2-D) VCSEL arrays make them particularly well suited for WDM applications. Multiple-wavelength VCSEL arrays have been demonstrated previously at short wavelengths [19], [20]. However, high-performance applications require long-wavelength (1.3–1.6 μm) sources. An externally optically pumped WDM VCSEL array operating at telecommunications wavelengths has been demonstrated [21], but independent direct channel modulation is preferred. In this work, wafer bonding was used to integrate GaAs–AlGaAs DBRs with a patterned InP–InGaAsP active region for direct electrical modulation of four independent wavelength channels. An intracavity superlattice consisting of alternating layers of InP and InGaAsP was selectively wet etched prior to wafer bonding in order to define lasing cavities with different wavelengths [21], as shown in Fig. 2. Each layer of the superlattice was 7.5 nm, leading to a wavelength spacing of approximately 5 nm for each layer removed. The wavelength spacing could be reduced to 2 nm by using thinner tuning layers, allowing for 16 channel transmission in the erbium-doped fiber amplifier (EDFA) C-band. An additional superlattice barrier was used to reduce the number of nonradiative recombination centers in the bonded active region [22], [23].

After bonding to the p-type GaAs–AlGaAs DBR, the InP substrate and InGaAsP etch stop are removed using wet etches. The second DBR, which is unintentionally doped, is then bonded under similar conditions to the exposed planar n-InP cladding. The finished device structure is shown in Fig. 3.

The top mirror is a 25.5-period p-type, parabolically graded GaAs–Al_{0.9}Ga_{0.1}As DBR, with an oxide aperture for mode and

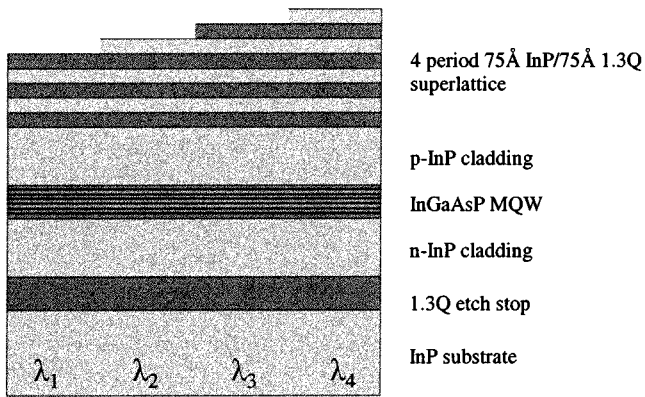


Fig. 2. Patterned InP-InGaAsP active region for a WDM VCSEL array.

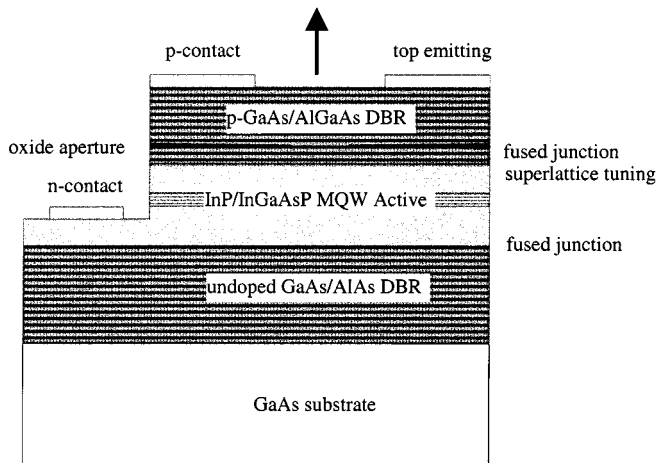


Fig. 3. Wafer-bonded, top-emitting VCSEL device structure.

current confinement. The 31-period bottom mirror is nonintentionally doped. The active region contains six strained InGaAsP quantum wells (QWs). The p-contact is on top of the p-DBR and the n-contact is on the n-cladding of the active region. Adjacent devices had different numbers of periods in the superlattice tuning layer. The device pitch was $250 \mu\text{m}$ in order to facilitate fiber coupling of multiple devices using standard components.

IV. DEVICE RESULTS

Voltage-current (V-I) characteristics were measured in order to determine that uniform bonding had been achieved. These curves are shown in Fig. 4 for four adjacent devices with an oxide aperture width of $5 \mu\text{m}$. Despite the nonplanar bonding and different numbers of superlattice periods, nearly uniform electrical characteristics were measured for four adjacent array elements. The high diode turn-on voltage is due to a voltage drop at the p-GaAs-p-InP bonded junction [9]. The differential resistance is roughly 320Ω . The resistance could be reduced by further optimizing the doping levels or by using two n-DBRs and tunnel junction injection.

Room-temperature light-current (L-I) characteristics are shown in Fig. 5 and spectra at a bias current of 6 mA are shown in Fig. 6 for four adjacent devices with an oxide aperture

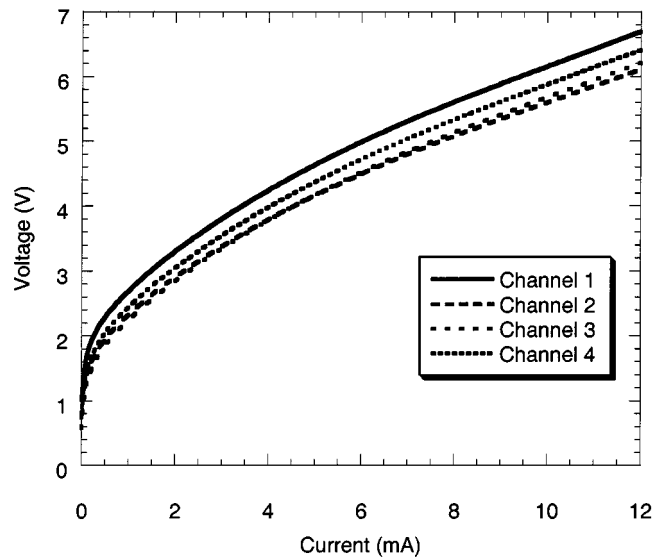


Fig. 4. Voltage-current characteristics of a WDM VCSEL array.

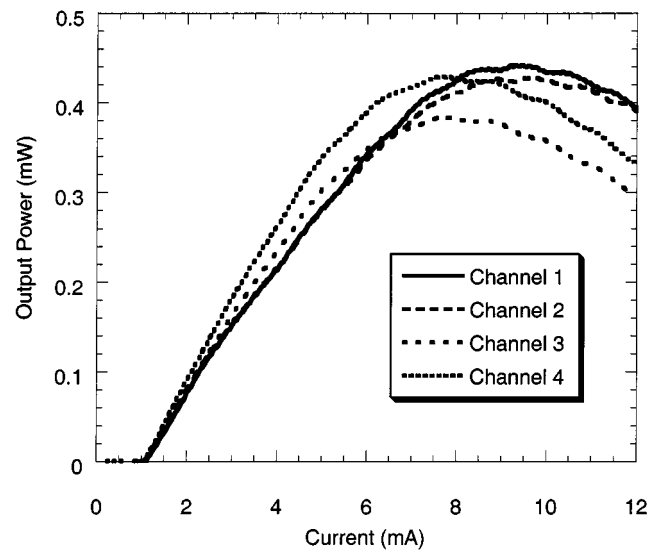


Fig. 5. CW L-I characteristics of a WDM VCSEL array.

width of $5 \mu\text{m}$. Variations in the curves can be attributed to the different mode-gain offsets of the channels. The lasing wavelengths are 1509.1, 1513.8, 1518.6, and 1524.4 nm. The active region photoluminescence peak is at 1542 nm. All four channels are on the short wavelength side of the gain peak. The higher numbered channels are located at longer wavelengths and are expected to have higher differential efficiencies. The exact wavelengths depend on the thickness of the superlattice tuning layers and the electrical power dissipated in each device. Increased control over the wavelength spacing is expected with improved superlattice growth and etch conditions.

Both the lasing wavelength and peak gain wavelength shift with temperature. The lasing wavelength increases at a rate of $0.1 \text{ nm}/^\circ\text{C}$ and the peak gain wavelength increases at a rate of $0.5 \text{ nm}/^\circ\text{C}$ [24]. Despite the unfavorable mode-gain offset, CW operation for individual devices was achieved at temperatures

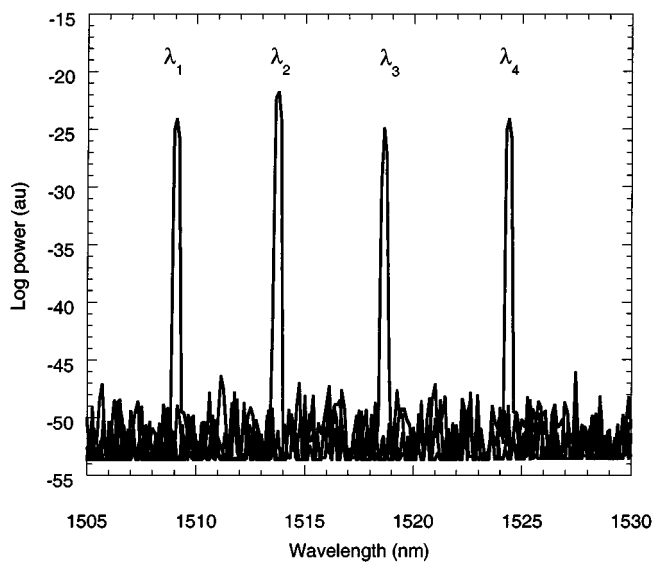


Fig. 6. Spectra of WDM VCSEL array at bias currents of 6 mA.

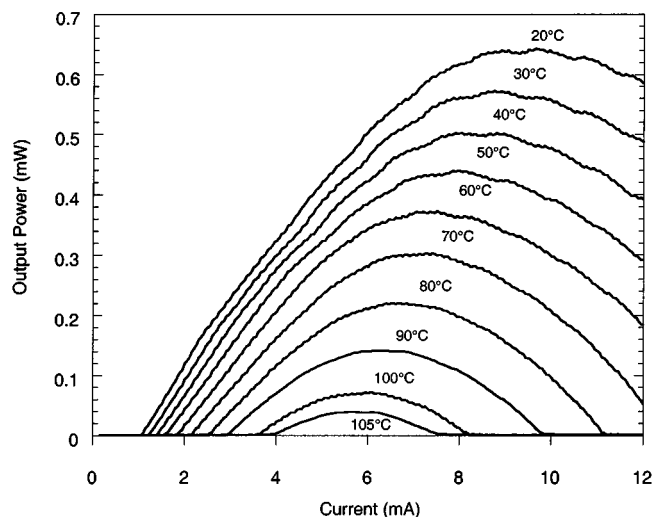


Fig. 7. CW $L-I$ characteristics of the 1525-nm device for ambient temperatures of 20 °C–105 °C.

as high as 105 °C. A family of $L-I$ curves for CW operation at ambient temperatures of 20 °C–105 °C is shown in Fig. 7. The devices were tested p-side up. The lasing wavelength is 1525 nm. This is the highest CW lasing temperature reported for an electrically pumped long-wavelength VCSEL.

The improved high-temperature operation compared to previously fabricated devices [23] is due to reduced diode turn-on voltage and lowered differential resistance. Previous devices were limited by poor electrical contacts. These improvements reduce the dissipated electrical power and device self-heating. A simple thermal analysis is shown in Fig. 8. The data points indicated by squares show the electrical power dissipated at the bias point where the $L-I$ characteristic have rolled over and the device is no longer lasing. Knowing that the maximum active region temperature (T_{max}) is equal to the ambient temperature

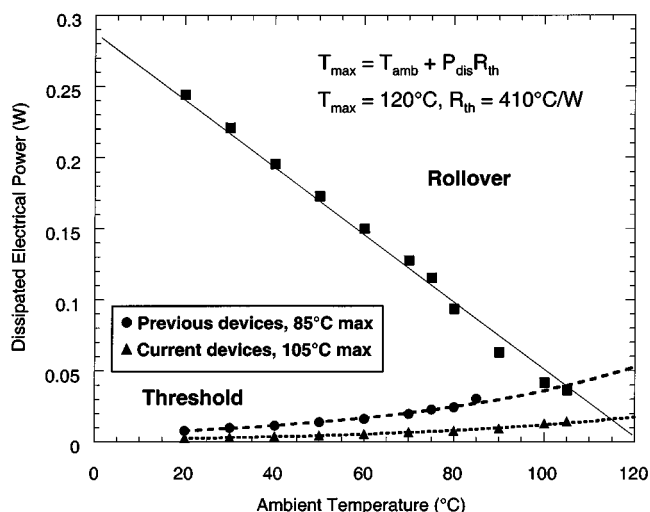


Fig. 8. Thermal comparison of previous and current devices.

(T_{amb}) plus the thermal resistance (R_{th}) multiplied by the dissipated electrical power (P_{dis}), a value of 120 °C is extracted by a linear fit. The data points indicated by circles show the electrical power dissipated at threshold by previously fabricated devices. The data points indicated by triangles show the electrical power dissipated at threshold by the device with the $L-I$ characteristics shown in Fig. 7. The two devices compared were fabricated using the same material and structure. They have identical thermal resistances of 410 °C/W and nearly identical amounts of power dissipated at rollover at the common operating temperatures. The CW operating regime for each device is bounded by the threshold and rollover dissipated power curves. The current generation of devices have threshold voltages of approximately 2.4 V, compared to the threshold voltage of 6.6 V reported earlier. The reduced threshold voltage dramatically decreases the amount of dissipated electrical power. The threshold curve now intersects the rollover curve at a higher ambient temperature. To summarize, device self-heating has been reduced so that the active region reaches the maximum lasing temperature at a higher ambient temperature. Improved high-temperature performance, including higher output powers over the operating temperature range, should be possible with improved mode-gain offset and reduced differential resistance.

Although the differential efficiency has been improved compared to previous devices (12% versus 9%), hole current spreading and nonuniform hole distribution in the QWs are still limiting factors [25]. The lack of a robust aperturing technique on InP forces placement of the oxide aperture in the GaAs–AlGaAs DBR. Hole current spreading at the bonded junction, superlattice layers, and through the p-doped InP creates a wider hole profile at the QWs than at the oxide aperture. Current crowding and spatial hole-burning also contribute to nonuniform injection. Simulation of these processes results in the calculated profiles shown in Fig. 9. The x axis shows the radial coordinate in micrometers, with 0 μm denoting the center of the device pillar. Current profiles are calculated at bias currents of 1.5 mA and 10 mA at the oxide aperture and at the first barrier. Significant current spreading is observed at both low and high bias currents. Current crowding is visible at the

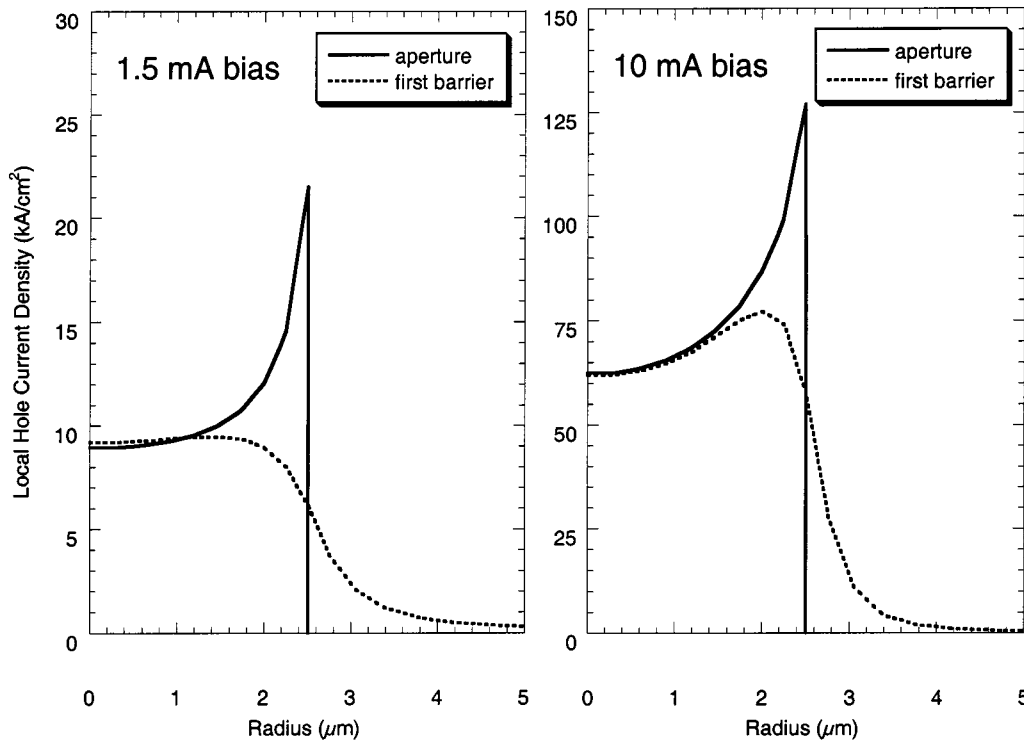


Fig. 9. Local hole current density distributions at oxide aperture and first active region barrier for bias currents of 1.5 and 10 mA.

oxide aperture even at low current densities. The combination of current crowding and spatial hole burning creates a highly nonuniform hole current profile in the active region for elevated bias currents. Improved current confinement techniques are being developed to mitigate these effects.

V. CONCLUSION

Four-channel WDM VCSEL arrays were fabricated using an intracavity superlattice tuning layer. The lasing wavelengths are 1509.1, 1513.8, 1518.6, and 1524.4 nm. The channel count can be increased by using thinner tuning layers, with the potential for 16-channel operation within the EDFA *C*-band. Individual devices exhibited excellent thermal performance, with CW lasing at temperatures as high as 105 °C.

The lower testing and packaging costs of VCSELs make these WDM arrays a potentially attractive alternative to DFB lasers for certain applications. Future work will include optimizing individual device performance, crosstalk measurements, and transmission experiments.

REFERENCES

- [1] M. C. Amann, M. Ortsiefer, R. Shau, G. Bohm, F. Kohler, M. Zigl-drum, and J. Robkopf, "High-performance vertical-cavity surface-emitting lasers for telecommunication wavelengths," in *26th Eur. Conf. Optical Communication*, Munich, Germany, 2000, postdeadline 3.3.
- [2] E. Hall, S. Nakagawa, G. Almuneau, J. Kim, D. Buell, and L. A. Coldren, "88°C, continuous-wave operation of 1.55 μm vertical-cavity surface emitting lasers," in *26th Eur. Conf. Optical Communication*, Munich, Germany, 2000, postdeadline 3.4.
- [3] J. Boucart, C. Starck, F. Gaborit, A. Plais, N. Bouche, E. Derouin, L. Goldstein, C. Fortin, D. Carpentier, P. Salet, F. Brillouet, and J. Jacquet, "1-mW CW-RT monolithic VCSEL at 1.55 μm," *IEEE Photon. Technol. Lett.*, vol. 11, pp. 629–631, 1999.
- [4] W. Yuen, G. S. Li, R. F. Nabiev, J. Boucart, P. Kner, R. J. Stone, D. Zhang, M. Beaudoin, T. Zheng, C. He, K. Yu, M. Jansen, D. P. Worland, and C. J. Chang-Hasnain, "High-performance 1.6 μm single-epitaxy top-emitting VCSEL," *Electron. Lett.*, vol. 36, pp. 1121–1123, 2000.
- [5] A. Karim, P. Abraham, D. Lofgreen, Y. J. Chiu, J. Piprek, and J. E. Bowers, "Wafer bonded long wavelength vertical cavity lasers with continuous wave operation up to 105°C," *Electron. Lett.*, submitted for publication.
- [6] V. Jayaraman, J. C. Geske, M. H. MacDougal, T. D. Lowes, F. H. Peters, D. VanDeusen, T. C. Goodnough, S. P. Kilcoyne, and D. Welch, "High temperature 1300 nm VCSEL's for single-mode fiber-optic communication," in *Proc. LEOS Summer Topical Meetings*, San Diego, CA, 1999, pp. 19–20.
- [7] J. F. Klem, O. Blum, and K. Lear, "Antimonide-based approaches for long-wavelength VCSELs," in *Proc. LEOS 1998*, vol. 2, San Francisco, CA, 1998, pp. 130–131.
- [8] E. Hall, G. Almuneau, J. K. Kim, O. Sjolund, H. Kroemer, and L. A. Coldren, "Electrically-pumped, single-epitaxial VCSEL's at 1.55 μm with Sb-based mirrors," *Electron. Lett.*, vol. 35, pp. 1337–1338, 1999.
- [9] A. Black, A. R. Hawkins, N. M. Margalit, D. I. Babic, A. L. Holmes, Jr., Y. L. Chang, P. Abraham, J. E. Bowers, and E. L. Hu, "Wafer fusion: Materials issues and device results," *IEEE J. Select. Topics Quantum Electron.*, vol. 3, pp. 943–951, 1997.
- [10] Z. H. Zhu, F. E. Ejeckam, Y. Qian, Z. Jizhi, Z. Zhenjun, G. L. Christenson, and Y. H. Lo, "Wafer bonding technology and its applications in optoelectronic devices and materials," *IEEE J. Select. Topics Quantum Electron.*, vol. 3, pp. 927–936, 1997.
- [11] L. Goldstein, C. Fortin, C. Starck, A. Plais, J. Jacquet, J. Boucart, A. Rocher, and C. Poussou, "GaAlAs/GaAs metamorphic Bragg mirror for long wavelength VCSELs," *Electron. Lett.*, vol. 34, pp. 268–270, 1998.
- [12] R. Shau, M. Ortsiefer, M. Zigl-drum, J. Roskopf, G. Bohm, F. Kohler, and M. C. Amann, "Low-threshold InGaAlAs/InP vertical-cavity surface-emitting laser diodes for 1.8 μm wavelength range," *Electron. Lett.*, vol. 36, pp. 1286–1287, 2000.
- [13] M. Ortsiefer, R. Shau, M. Zigl-drum, G. Bohm, F. Kohler, and M. C. Amann, "Submilliamp long-wavelength InP-based vertical-cavity surface-emitting laser with stable linear polarization," *Electron. Lett.*, vol. 36, pp. 1124–1126, 2000.

[14] S. Adachi, "Lattice thermal resistivity of III-V compound alloys," *J. Appl. Phys.*, vol. 54, pp. 1844-1848, 1983.

[15] J. M. Dallesasse, N. Holonyak, Jr., A. R. Sugg, T. A. Richard, and N. El-Zein, "Hydrolyzation oxidation of Al/sub x /Ga/sub $1 - x$ /As-AlAs-GaAs quantum well heterostructures and superlattices," *Appl. Phys. Lett.*, vol. 57, pp. 2844-2846, 1990.

[16] D. L. Huffaker, D. G. Deppe, K. Kumar, and T. J. Rogers, "Native-oxide defined ring contact for low threshold vertical-cavity lasers," *Appl. Phys. Lett.*, vol. 65, pp. 97-99, 1994.

[17] D. I. Babic, K. Streubel, R. P. Mirin, N. M. Margalit, J. E. Bowers, E. L. Hu, D. E. Mars, Y. Long, and K. Carey, "Room-temperature continuous-wave operation of 1.54- μm vertical-cavity lasers," *IEEE Photon. Technol. Lett.*, vol. 7, pp. 1225-1227, 1995.

[18] N. M. Margalit, D. I. Babic, K. Streubel, R. P. Mirin, R. L. Naone, J. E. Bowers, and E. L. Hu, "Submilliamp long wavelength vertical cavity lasers," *Electron. Lett.*, vol. 32, pp. 1675-1677, 1996.

[19] D. L. Huffaker and D. G. Deppe, "Multiwavelength, densely-packed 2x2 vertical-cavity surface-emitting laser array fabricated using selective oxidation," *IEEE Photon. Technol. Lett.*, vol. 8, pp. 858-860, July 1996.

[20] Y.-G. Ju, D. Lofgreen, A. Fiore, S.-Y. Hu, E. Hegblom, D. Loderback, O. Sjolund, A. Huntington, and L. A. Coldren, "Densely packed pie shaped vertical-cavity surface-emitting laser array incorporating a tapered one-dimensional wet oxidation," *IEEE Photon. Technol. Lett.*, vol. 12, pp. 462-464, 2000.

[21] V. Jayaraman and M. Kilcoyne, "WDM array using long-wavelength vertical cavity lasers," *Proc. SPIE*, vol. 2690, pp. 325-336, 1996.

[22] K. A. Black, P. Abraham, A. Karim, J. E. Bowers, and E. L. Hu, "Improved luminescence from InGaAsP/InP MQW active regions using a wafer fused superlattice barrier," in *Proc. Indium Phosphide and Related Materials*, Davos, Switzerland, 1999, pp. 357-360.

[23] A. Karim, K. A. Black, P. Abraham, D. Lofgreen, Y. J. Chiu, J. Piprek, and J. E. Bowers, "Superlattice barrier 1528 nm vertical cavity laser with 85°C continuous wave operation," *IEEE Photon. Technol. Lett.*, vol. 12, pp. 1438-1440, Nov. 2000.

[24] J. Piprek, Y. A. Akulova, D. I. Babic, L. A. Coldren, and J. E. Bowers, "Minimum temperature sensitivity of 1.55 μm vertical-cavity lasers at -30 nm gain offset," *Appl. Phys. Lett.*, vol. 72, pp. 1814-1816, 1998.

[25] J. Piprek, P. Abraham, and J. E. Bowers, "Carrier nonuniformity effects on the internal efficiency of multiquantum-well lasers," *Appl. Phys. Lett.*, vol. 74, pp. 489-491, 1999.



Patrick Abraham (M'99-SM'99) received the MS and Ph.D degrees in materials science from the University Claude Bernard Lyon 1, Lyon, France, in 1984 and 1987, respectively.

He was a Researcher at Centre National de la Recherche Scientifique (CNRS) and worked until 1995 for the Laboratoire de Physico-Chimie Minérale in France. His work interests there included the fundamental aspect of metal-organic chemical vapor disposition (MOCVD) growth: precursor pyrolysis, surface reaction, and new precursor evaluation. He then joined University of California at Santa Barbara as a Research Engineer, where until 1999 his research interests included laser active region design, MOCVD growth, compliant substrates, and wafer fusing. He is now Manager of the MOCVD group at Agility Communications.

Dan Lofgreen (S'97), photograph and biography not available at the time of publication.



Yi-Jen Chiu (S'93-M'96) received the B.S. degree from National Chengkung University, Tainan, Taiwan, the M.S degree from National Taiwan University, Taipei, Taiwan, and the Ph.D. degree in electrical engineering from the University of California at Santa Barbara, in 1989, 1992, and 1999, respectively.

His current research interests involve material characterization, device design, and fabrication for high-speed InAlGaAs-InP and InGaAs-InP traveling wave electro-absorption modulators, molecular beam epitaxy growth of nonstochastic low-temperature GaAs and AlGaAs material for photodetectors, and vertical-cavity surface-emitting lasers.



Adil Karim (S'97), received the B.S. degree in applied physics from the California Institute of Technology, Pasadena, CA, the M.S. degree in optics from the University of Rochester, Rochester, NY, and the Ph.D. degree in electrical engineering from the University of California at Santa Barbara, in 1996, 1997, and 2001, respectively.

He is currently a Test Engineer at Agility Communications, Santa Barbara, CA. His research interests include vertical-cavity lasers, tunable lasers, and wavelength-division multiplexing.



Joachim Piprek (M'94-SM'98), received the Ph.D. degree in solid state physics from Humboldt University, Berlin, Germany, in 1986.

He worked in industry and academia on design and analysis of optoelectronic devices. He currently is an Adjunct Associate Professor, University of California at Santa Barbara, Santa Barbara, CA. His research interests include in-plane and vertical-cavity lasers, novel semiconductor materials, and advanced computer simulation.



John E. Bowers (S'78-M'81-SM'85-F'93) received the M.S. degree and the Ph.D. degree in applied physics from Stanford University, Stanford, CA.

He is Director of the Multidisciplinary Optical Switching Technology Center (MOST), and a Professor in the Department of Electrical Engineering, University of California at Santa Barbara, (UCSB). He is a member of the Optoelectronics Technology Center and the NSF Science and Technology Center on Quantized Electronic Structures. His research interests are primarily concerned with high-frequency optoelectronic devices and physics. He was with AT&T Bell Laboratories and Honeywell before joining UCSB. He has published five book chapters, over 200 journal papers, over 200 conference papers and holds 12 patents. Dr. Bowers is a fellow of the American Physical Society. He is a recipient of Sigma Xi's Thomas F. Andrew prize and the NSF Presidential Young Investigator Award and NSF Graduate Fellowship.

Dr. Bowers is a recipient of the IEEE LEOS William Streifer Award, and is Vice President for Conferences of IEEE LEOS.